3.2 Proton-Proton Scattering at T_L = 500 - 1090 MeV

Abstract. The p-p elastic scattering amplitudes at T_L = 500–1090 MeV are determined by phase-shift analyses using the K-matrix parametrization proposed by the VPI group. In addition to the previously suggested waves $^1D_2$,$^3F_3$,$^3P_2$ and $^1G_4$ for dibaryon, the amplitude of the $^3H_5$-wave shows a narrow resonance-like behaviour.

(Prog. Theor. Phys. **95** (1996), 691.)

Spin polarized experiments in nucleon-nucleon system have revealed various problems from the early study of nuclear force. The research of dibaryon and the study of threshold effect of the inelastic processes of p-p scattering have been studied at intermediate energies vigorously by many groups and, for these projects, a large number of the experimental data on spin observables have been accumulated. In our previous paper, we reported the scattering amplitudes determined by phase-shit analyses (PSA) of p-p elastic scattering between 500 and 800 MeV[42] at several energy points for which the situation of the experimental data was considered to be close to the so-called "complete experiments"[65], In this paper, we report the results of a new phase shift analysis adopting the VPI K-matrix parametrization[30, 66], since it enables us to have more stable mixing amplitudes relative to the ones in our previous parametrization. In the VPI parametrization the partial wave S-matrix is given by

$$S = \frac{1 + iK}{1 - iK} \tag{3.12}$$

and for the singlet state and the uncoupled triplet state, K is represented as

$$K = \tan\delta + i\tan^2\rho \tag{3.13}$$

For the coupled triplet states, the K-matrix is taken as

$$K = \begin{bmatrix} K_{r-} & K_{r0} \\ K_{r0} & K_{r+} \end{bmatrix} + i\begin{bmatrix} \tan^2\rho_- & \tan\rho_-\tan\rho_+ \\ \tan\rho_-\tan\rho_+ & \tan^2\rho_+ \end{bmatrix}, \tag{3.14}$$

$$K_{r\pm} = \frac{\sin(\delta_+ + \delta_-) \pm \cos(2\epsilon)\sin(\delta_+ - \delta_-)}{\cos(\delta_+ + \delta_-) + \cos(2\epsilon)\sin(\delta_+ - \delta_-)}, \tag{3.15}$$

$$K_{r0} = \frac{\sin(2\epsilon)}{\cos(\delta_+ + \delta_-) + \cos(2\epsilon)\cos(\delta_+ - \delta_-)}. \tag{3.16}$$

Here $\delta_\pm = \delta_{J\pm1,J}$, $\rho_\pm = \rho_{J\pm1,J}$ and ϵ is the mixing parameter.

The number of experimental data used in the present analyses above 800 MeV are shown in Table 3.5[67]. Below 800MeV, the data base of PSA is almost the same as the previous ones[42].

Recently, precise experiments of the $d\sigma/d\Omega$ of p-p scattering have been carried out at LAMPF[68]. These data are added to the data base at T_L = 500, 630 and 730 MeV. Considerable systematic measurements of the polarization (P) and the complex double and triple spin correlation parameters have been measured at SATURNE II above 800 MeV[69]. All of these data are used in the present analyses. We also supplement the data base by using pseudo-data made by using the same method (spline-function) as in Ref. [42] on the forward and several other observables. The numbers of the pseudo-data are shown to be asterisked in Table 3.5.

Table 3.5: The observables and their numbers of the experimental data used in the phase-shift analysis at each energy[42].

T_L (MeV)	830(20)	870(20)	930(20)	990(20)	1090 (20)
Forward Obs.[a)]	7(*4)	7(*4)	7(*4)	7(*4)	7(*4)
$d\sigma/d\Omega$	105(*15)	148(*8)	115(*15)	285	98(*15)
P	186(*11)	215(*11)	199(*11)	221(*11)	73(*11)
R				10	
A				10	
D	12	14	10	22	14
D_{LS}	12	16	12	12	14
A_{NN}	25	56	25	33	36
A_{LL}	28	80	14	34	38
A_{SL}	19	35	12	13	31
K_{NN}	6	7	5	6	7
K_{LS}	6	16	6	6	7
H_{LNS}				3	
$A_{LL}+\delta A_{SL}$	21				
$P+\delta A_{SL}$	22	22	23	23	22
$K_{LS}+\alpha K_{SS}+\beta K_{LL}$	7	7	5	4	7
$H_{LLN}+\beta K_{LL}$	5	8	5	5	7
$H_{NLS}+\alpha K_{SS}$	5	8	6	5	6
$H_{LNS}+\alpha H_{SNS}+\beta K_{LL}$	6	7	5	3	6
$K_{NN}+\alpha H_{SLN}+\beta K_{SL}+\gamma H_{NLL}$	5	8	6	5	6

a) Forward Obs.: $\sigma_t, \sigma_r, \Delta\sigma_T, \Delta\sigma_L, \alpha$, Re$F_2$, Re$F_3$

There has been a controversy concerning the coupling constant $g_{\pi NN}$ for the last decade. In the present analyses $g_{\pi NN}$=13.75 is used[70]. Phase shifts and χ^2-values obtained by the present PSA are listed in Table 3.6. We could have stable amplitudes of p-p scattering below 580 MeV and 800 MeV and also obtain almost stable solutions above 800 MeV by using the data base supplemented by the pseudo-data which reflect an energy dependence of each observable by spline-interpolation of the experimental data. Therefore one can see that the experiments for such observables as $d\sigma/d\Omega$ at θ_c=20$\sim$40° and P at $\theta_c \leq 30°$ lead to stable solution.

The Argand diagrams of the obtained partial-wave amplitudes which show a resonance-like behaviour are shown in Figs. 3.4(a)$\sim$(c). These diagrams are almost the same as the results of our previous PSA below 800 MeV in which a different S-matrix parametrization was used.

Using the obtained partial wave amplitudes, we evaluate the resonance parameters of each wave by means of the distorted-wave Born approximation with smooth background amplitudes as follows,

$$T = \frac{S_B - 1}{2i} + \sqrt{S_B}\frac{x\Gamma/2}{\sqrt{S} - \sqrt{S_R} + i\Gamma/2}\sqrt{S_B}\exp[-\{(\sqrt{s} - \sqrt{s_R})/\Gamma_\gamma\}^2], \qquad (3.17)$$

Table 3.6: Phase-shift solutions and χ^2-values at each energy.

T_L (MeV)	500		530		560	
	$\chi^2/N_t^{b)}$=1038/459		χ^2/N_t=679/348		χ^2/N_t=635/379	
Partial waves	δ	ρ	δ	ρ	δ	ρ
$^1S_0$	−23.56 ± 0.36	5.23 ± 0.24	−25.46 ± 0.13	0.49 ± 0.31	−27.99 ± 0.65	2.40 ± 0.42
$^3P_0$	−27.93 ± 0.37	9.81 ± 0.21	−29.74 ± 0.12	11.83± 0.10	−33.58 ± 0.54	19.45 ± 0.18
$^3P_1$	−41.71 ± 0.47	12.00 ± 0.18	−42.98 ± 0.08	18.23 ± 0.06	−43.80 ± 0.79	17.36 ± 0.21
$^3P_2$	17.24 ± 0.17	6.38 ± 0.16	17.18 ± 0.02	5.49 ± 0.06	18.13 ± 0.34	5.99 ±0.21
ϵ_2	−0.86 ± 0.34		−0.51 ± 0.23		−0.74 ± 0.25	
$^1S_0$	13.20 ± 0.08	14.26 ± 0.10	12.18± 0.06	17.12 ± 0.04	12.04 ± 0.11	19.07± 0.10
$^3S_0$	−0.85 ± 0.12	0.60 ± 0.14	−1.11 ± 0.07	0.52 ± 0.08	−1.27 ± 0.24	0.92 ± 0.14
$^3S_0$	−1.90 ± 0.12	7.65 ± 0.07	−0.84 ± 0.03	10.01 ± 0.03	−0.12 ± 0.15	11.93 ± 0.08
$^3S_0$	4.12 ± 0.08	0.00 ± 0.23	3.85 ± 0.04	0.09 ± 0.27	4.70 ± 0.09	0.00 ± 0.75
ϵ_4	−1.71± 0.26		−1.43 ± 0.19		−1.64 ± 0.18	
$^1S_0$	2.84 ± 0.05	5.41 ± 0.07	3.30 ± 0.02	5.37 ± 0.04	3.48 ± 0.05	5.38 ± 0.07
$^3S_0$	0.63 ± 0.05	1.11 ± 0.17	0.39 ± 0.04	0.01 ± 0.27	0.75 ± 0.07	0.02 ± 0.36
$^3S_0$	−1.38 ± 0.07	0.02 ± 0.68	−1.65 ± 0.04	0.41 ± 0.12	−2.07 ± 0.08	0.01 ± 0.62
$^3S_0$	1.00 ± 0.04	0.36 ± 0.27	1.36 ± 0.27	0.08 ± 0.12	1.18 ± 0.04	0.32 ± 0.24
T_L (MeV)	580		630		730	
	χ^2/N_t=959/456		χ^2/N_t=1090/522		χ^2/N_t=1031/462	
$^1S_0$	−28.86 ± 0.24	0.59 ± 0.43	−35.46± 0.09	8.10 ± 0.10	−42.90 ± 0.26	13.64 ± 0.12
$^3S_0$	−32.71 ± 0.24	12.50 ± 0.11	−40.49 ± 0.19	25.57 ± 0.07	−42.93 ± 0.33	24.47 ± 0.08
$^3S_0$	−44.67 ± 0.26	13.05 ± 0.12	−50.28 ± 0.09	23.69 ± 0.06	−52.67 ± 0.13	23.72 ± 0.07
$^3S_0$	18.76 ± 0.10	13.24 ± 0.07	17.71 ± 0.06	13.67 ± 0.04	15.20 ± 0.09	19.89 ± 0.05
ϵ_2	−0.30 ± 0.26		0.86 ± 0.16		1.46 ± 0.26	
$^1S_0$	11.12 ± 0.05	20.57 ± 0.05	8.51 ± 0.04	21.69 ± 0.03	4.54 ± 0.29	23.43 ± 0.06
$^3S_0$	−1.26 ± 0.06	1.16 ± 0.06	−3.02 ± 0.05	1.14 ± 0.15	−5.21 ± 0.07	4.29± 0.04
$^3S_0$	0.13 ± 0.07	13.04 ± 0.04	0.43 ± 0.04	16.02 ± 0.04	−1.09 ± 0.13	24.07 ± 0.05
$^3S_0$	4.57 ± 0.05	0.16 ± 0.27	5.31 ± 0.02	0.03 ± 0.11	5.61 ± 0.05	5.91 ± 0.07
ϵ_4	−1.63 ± 0.19		−1.30 ± 0.16		−1.38 ± 0.20	
$^1S_0$	3.67 ± 0.04	4.69 ± 0.04	3.80 ± 0.02	4.21 ± 0.04	4.49 ± 0.08	4.99 ± 0.10
$^3S_0$	0.71 ± 0.04	0.02 ± 0.40	0.77 ± 0.04	1.55 ± 0.07	−0.11 ± 0.05	0.81 ± 0.06
$^3S_0$	−1.59 ± 0.06	1.41 ± 0.08	−1.28 ± 0.08	4.82 ± 0.06	−0.92 ± 0.08	7.80 ± 0.06
$^3S_0$	1.33 ± 0.02	0.10 ± 0.14	1.25 ± 0.03	0.19 ± 0.15	1.83 ± 0.07	0.17 ± 0.10

b):Total number of the used data in PSA.

where S_B, $\sqrt{S_R}$, Γ and x are the background amplitude, the resonance mass, the total width and the elasticity. Γ_γ is a parameter of the cutoff factor. The evaluated values of the resonance paremeters are given in Table 3.7. The values for $^1D_2$,$^3F_3$,$^3P_2$ and $^1G_4$ are close to those previously cited by certain groups. The amplitudes of the $^3H_5$-wave may be found to have a narrow resonance-like behaviour, which was suggested by Nagata et al.[72]. The calculated values using Eq.(3.17) with the values of Table 3.7 are shown in Fig. 3.4. The values of the parameters are close to the ones given in Ref. [72]. As can be seen in this figure, the results of several other groups show the same tendencies as the present one. In spite of these consistencies, the experimental data at 600∼800 MeV do not seem to be good enough to draw a definite conclusion. Further accumulation of accurate experimental data for *p*-*p* scattering in this energy region is desired for resolving the narrow-dibaryon problem.

Table 3.6: (Continued.)

T_L (MeV)	800		830		870	
	χ^2/N_t=2518/1014		χ^2/N_t=610/456		χ^2/N_t=972/675	
Partial waves	δ	ρ	δ	ρ	δ	ρ
$^1S_0$	-50.63 ± 0.13	27.36 ± 0.08	-56.96 ± 0.31	36.90 ± 0.10	-58.77 ± 0.31	37.03 ± 0.11
$^3P_0$	-49.81 ± 0.09	29.56 ± 0.07	-47.50 ± 0.20	29.19 ± 0.06	-49.05 ± 0.44	32.63 ± 0.09
$^3P_1$	-55.01 ± 0.05	25.83 ± 0.05	-53.09 ± 0.11	23.14 ± 0.05	-54.44 ± 0.14	21.68 ± 0.06
$^3P_2$	12.43 ± 0.04	21.89 ± 0.03	11.51 ± 0.07	24.38 ± 0.05	10.43 ± 0.15	26.74 ± 0.05
ϵ_2	1.65 ± 0.03		1.27 ± 0.03		1.92 ± 0.03	
$^1D_2$	4.56 ± 0.07	24.27 ± 0.02	3.64 ± 0.08	24.31 ± 0.04	0.69 ± 0.07	23.97 ± 0.03
$^3F_2$	-6.30 ± 0.05	5.42 ± 0.02	-5.31 ± 0.08	5.89 ± 0.05	-5.39 ± 0.07	6.16 ± 0.04
$^3F_3$	-4.28 ± 0.06	26.18 ± 0.03	-6.62 ± 0.04	27.45 ± 0.04	-10.86 ± 0.08	25.59 ± 0.10
$^3F_4$	6.60 ± 0.02	4.47 ± 0.04	7.07 ± 0.03	9.41 ± 0.06	7.47 ± 0.04	10.35 ± 0.03
ϵ_4	-1.52 ± 0.02		-1.71 ± 0.02		-2.51 ± 0.02	
$^1G_4$	3.94 ± 0.02	5.41 ± 0.03	3.85 ± 0.02	6.92 ± 0.04	3.21 ± 0.03	8.09 ± 0.02
$^3H_4$	0.99 ± 0.02	4.27 ± 0.03	1.54 ± 0.05	1.53 ± 0.06	1.81 ± 0.04	0.16 ± 0.03
$^3H_5$	-1.38 ± 0.01	8.31 ± 0.02	-1.30 ± 0.02	10.47 ± 0.05	-1.50 ± 0.04	10.33 ± 0.03
$^3H_6$	1.74 ± 0.02	1.34 ± 0.07	1.74 ± 0.03	0.56 ± 0.09	1.55 ± 0.04	0.88 ± 0.03
ϵ_6	-1.17 ± 0.02		-1.06 ± 0.01		-1.23 ± 0.02	
$^1I_6$	1.43 ± 0.03	0.08 ± 0.24	1.54 ± 0.01	0.44 ± 0.07	2.09 ± 0.02	4.36 ± 0.02
T_L (MeV)	930		990		1090	
	χ^2/N_t=676/453		χ^2/N_t=1690/710		χ^2/N_t=590/379	
$^1S_0$	-54.19 ± 0.20	28.41 ± 0.06	-53.77 ± 0.23	20.28 ± 0.08	-61.68 ± 0.34	18.73 ± 0.11
$^3P_0$	-50.18 ± 0.25	35.55 ± 0.06	-51.95 ± 0.21	30.91 ± 0.06	-48.28 ± 0.49	42.14 ± 0.09
$^3P_1$	-53.68 ± 0.11	24.94 ± 0.05	-54.51 ± 0.08	18.98 ± 0.07	-55.36 ± 0.14	14.81 ± 0.09
$^3P_2$	6.41 ± 0.07	25.83 ± 0.04	4.27 ± 0.11	28.61 ± 0.04	6.07 ± 0.19	34.71 ± 0.05
ϵ_2	1.91 ± 0.02		2.30 ± 0.02		2.94 ± 0.04	
$^1D_2$	0.67 ± 0.03	25.89 ± 0.05	0.64 ± 0.03	26.76 ± 0.04	0.49 ± 0.12	29.29 ± 0.04
$^3F_2$	-7.28 ± 0.04	6.05 ± 0.05	-6.48 ± 0.05	7.35 ± 0.04	-2.32 ± 0.13	7.44 ± 0.05
$^3F_3$	-13.25 ± 0.04	28.81 ± 0.03	-10.91 ± 0.07	28.56 ± 0.04	-15.02 ± 0.13	26.68 ± 0.06
$^3F_4$	7.94 ± 0.03	11.88 ± 0.05	7.10 ± 0.04	10.98 ± 0.05	7.18 ± 0.09	8.99 ± 0.06
ϵ_4	-2.43 ± 0.01		-2.18 ± 0.01		-2.19 ± 0.02	
$^1G_4$	3.74 ± 0.01	9.59 ± 0.04	3.86 ± 0.01	11.04 ± 0.04	3.44 ± 0.04	11.95 ± 0.05
$^3H_4$	1.75 ± 0.03	1.03 ± 0.05	0.66 ± 0.04	2.96 ± 0.05	-0.88 ± 0.07	0.20 ± 0.08
$^3H_5$	-1.66 ± 0.01	10.51 ± 0.05	-2.67 ± 0.03	12.18 ± 0.05	-1.42 ± 0.07	13.85 ± 0.06
$^3H_6$	2.11 ± 0.02	2.80 ± 0.06	2.17 ± 0.02	1.23 ± 0.08	2.29 ± 0.07	5.01 ± 0.07
ϵ_6	-1.43 ± 0.01		-1.39 ± 0.01		-1.33 ± 0.02	
$^1I_6$	2.18 ± 0.01	2.99 ± 0.05	2.04 ± 0.01	4.86 ± 0.05	2.17 ± 0.03	4.13 ± 0.06

Table 3.7: The resonance parameters of possible dibaryons.

Partial waves	$\sqrt{s_R}$ (MeV)	Γ (MeV)	x	Γ_r (MeV)
$^3P_2$	2200	100	0.06	100
$^1D_2$	2155	120	0.10	120
$^3F_3$	2195	100	0.15	100
$^1G_4$	2230	80	0.03	80
$^3H_5$	2190	10	0.02	8

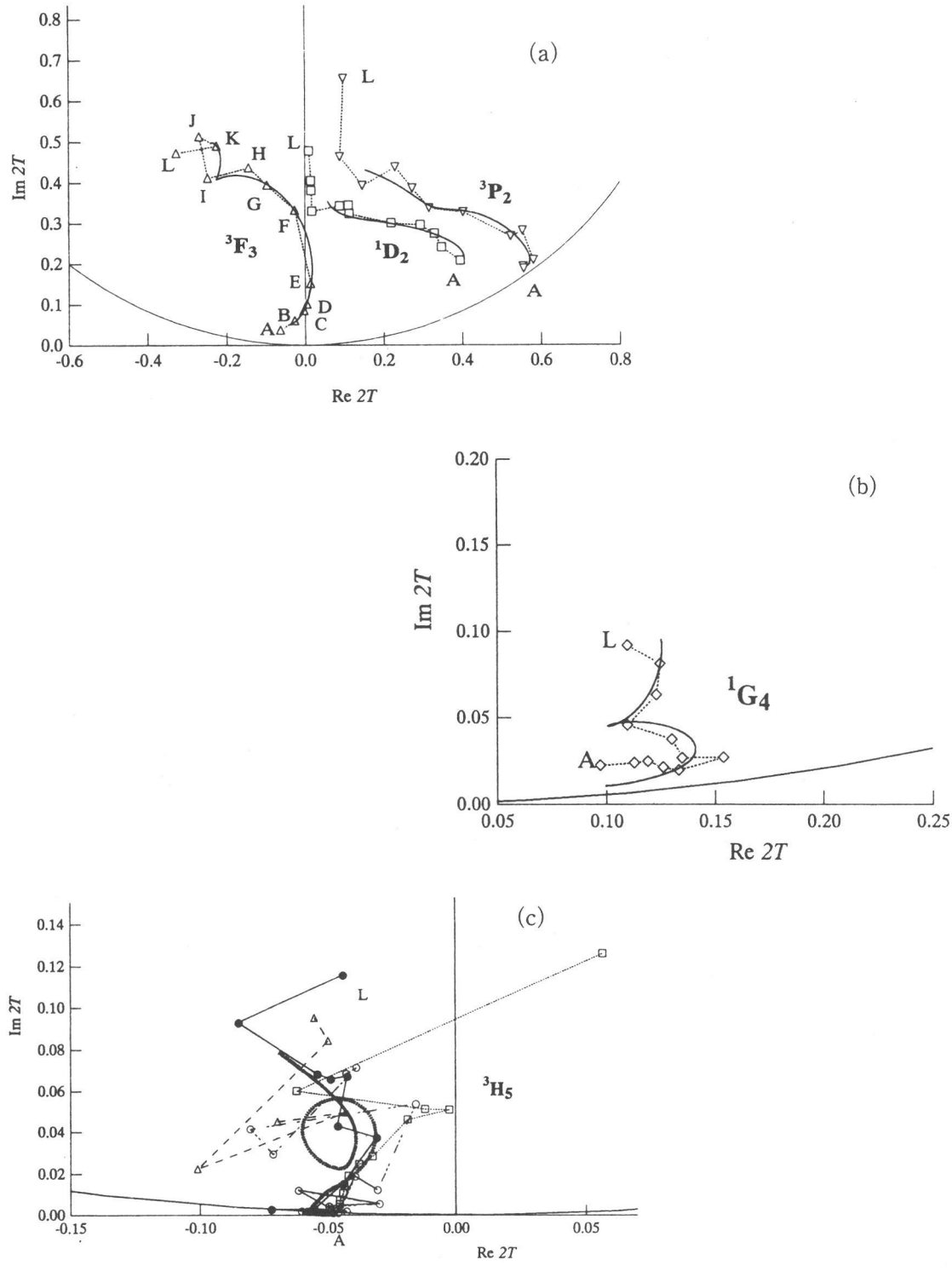

Figure 3.4: The Argand diagrams of partial wave amplitudes of the solutions obtained by the present PSA at 500(A), 530(B), 560(C), 580(D), 630(E), 730(F), 800(G), 830(H), 870(I), 930(J), 990(K) and 1090 MeV (L). Also the calculation with the resonance formula of Eq. (3.17) (solid-line in Figs. 3.4(a) and (b), bold-dotted line in (c)) are given using the values in Table 3.7. In Fig. 3.4(c), the results of PSA obtained by other groups(○:Higuchi et al.[10];△:Bystricky et al.[11]; □:SAID[71]) are shown together with the present one(●).